IEEE Access
Multidisciplinary | Rapid Review | Open Access Journal

Received July 23, 2019, accepted August 9, 2019, date of publication August 16, 2019, date of current version August 30, 2019.

Digital Object Identifier 10.1109/ACCESS.2019.2935780

Tunable Frequency-Selective Rasorber Based on Varactor-Embedded Square-Loop Array

YIHAO WANG[1], SHI-SHAN QI[1], (Member, IEEE), ZHONGXIANG SHEN[2], (Fellow, IEEE), AND WEN WU[1], (Senior Member, IEEE)

[1]School of Electronic and Optical Engineering, Nanjing University of Science and Technology, Nanjing 210094, China
[2]School of Electrical and Electronic Engineering, Nanyang Technological University, Singapore 639798

Corresponding author: Shi-Shan Qi (qishishan@gmail.com)

This work was supported in part by the National Natural Science Foundation of China under Grant 61771242.

ABSTRACT This paper presents a varactor-based tunable frequency-selective rasorber (FSR) with embedded bias grid. The proposed structure consists of a lossy layer based on square-loop arrays and a lossless layer. Each layer has an embedded wire grid that provides the bias voltage for the varactors through metallic vias. This arrangement can avoid unnecessary effects associated with the additional biasing network. An equivalent circuit model is developed to explain how the structure can provide a tunable transmission window within the absorption band. Simple design guidelines for the tunable FSR are then provided. The performance of the proposed structure is measured in a parallel-plate waveguide setup. Both simulated and measured results show that by changing the bias voltage from 16 to 4 V, the center transmission frequency of the FSR can be tuned from 5.2 to 3.8 GHz continuously. The insertion loss of the FSR within the transmission window is only 0.59 dB at 5.2 GHz and a fractional bandwidth of 93.1% (2.4–6.58 GHz) for −10 dB reflectivity is achieved under the normal incidence.

INDEX TERMS Frequency-selective surface, rasorber, reconfigurable rasorber, tunable absorber.

I. INTRODUCTION

Frequency-selective rasorber (FSR) has attracted growing attention due to its unique transmission and absorption characteristics [1]. Designed as a combination of frequency selective surface (FSS) and absorber, FSR can be transparent to incident electromagnetic (EM) waves in the passband and absorptive outside the passband, rather than reflective for conventional FSSs [2]. The key benefit of FSR is its suitability for stealthy radomes, which require a transmission window and a low radar cross section (RCS) over a desired frequency band. The rasorbers also have potential application in the protection and interference-mitigation of wireless local area network systems.

A conventional method of designing FSR structures is based on multi-layered frequency selective surfaces (FSSs) combined with lossy components or materials [4]–[12]. In the past, most of the existing configurations can only achieve one-sided absorption band (either lower or upper) [13]–[16]. To address this issue, a new concept of 3-D rasorbers was proposed in [17]–[20] to achieve a transmission window within a wide absorption band. In addition, the idea of bypassing the lossy components by adding resonators to improve the insertion loss within the transmission band was implemented in [21].

It is a challenging task to design a tunable and highly selective transmission window within a wide absorption band, or tunable FSR in short, though such tunable FSR can be very useful for many military systems. A tunable FSR based on 3-D structure was proposed in [22], though there were not experimental results reported. As for 2-D structures, based on existing tunable frequency-selective surfaces (FSSs), various methods of designing tunable FSRs can be proposed, such as using mechanical deformation [23], utilizing micro-electromechanical (MEMS) switches [24], magnetically tunable ferrite substrate [25], and liquid crystal [26]. However, the mechanical deformation method and MEMS switches have the disadvantages of being complicated structure and requiring large control voltage. It is also noted that the tuning ranges of the structures based on magnetically biased ferrite and liquid crystal are relatively limited.

A well-known technique of designing tunable FSSs is to use components such as varactors and PIN diodes [27]–[30]. They can provide electronic tuning with high-speed and

The associate editor coordinating the review of this article and approving it for publication was Vincenzo Conti.

exhibit wideband tuning range. Several designs of active FSR based on varactors and PIN diodes have been proposed so far, such as [31], [32]. However, the switchable FSR structure proposed in [31] can only provide one passband or none. Meanwhile, the insertion loss of the FSR reported in [32] is relatively large, and the filtering responses of the absorption band are not stable. In addition, it is desirable to avoid the use of complicated biasing network in these diode-based FSRs. According to [30], adding the extra biasing network and elements affects the frequency response of the original FSR. And the strategies for RF/DC isolation should also be considered.

In order to overcome the above issues, we present a double-layer varactor-based tunable FSR with two absorption bands at both sides of the transmission window in this paper. The lossy layer is achieved by utilizing a square-loop array combined with lumped resistors to provide the absorption band. A typical bandpass FSS layer is utilized to realize the transmission window within the absorption band. Both layers are constructed with varactors to achieve the coordinated tunable characteristic. The varactors in the front and back layers are connected to the ground through metallic vias and wire grids, which are incorporated with the biasing network and embedded in the FSS layers. Based on the presented equivalent circuit model (ECM), the tunable resonance and operating principle of the structure are analyzed in detail. This configuration can realize electronic tunability continuously with simple control of the bias voltage.

This paper is organized as follows. In Section II, we first describe the tunable FSR structure and its ECM to explain the operating principle. The detailed description of the tuning mechanism is also provided. Simple design guidelines are developed to implement the square-loop array-based tunable rasorber. After that, based on the method described above, an example of the tunable rasorber is designed. In Section III, the proposed tunable FSR is experimentally verified and discussed. A good agreement is observed between the measurement and simulation results. Finally, concluding remarks are given in Section IV.

II. ANALYSIS AND DESIGN OF THE TUNABLE FSR

A. DESCRIPTION OF THE TUNABLE RASORBE

In many FSR applications, the transmission window within the absorption band should can be adjusted according to the system requirements. A tunable rasorber can be designed by using varactors. Based on the reported designs [4], [6], [11], the unit cell configuration of our proposed tunable FSR is shown in Fig. 1. The structure contains one lossy FSS layer placed above a lossless FSS layer with a separation of a quarter-wavelength air spacer. It is well known that the lossy layer can be implemented by either resistive sheet or resistor-loaded FSS. The incoming EM wave can propagate through the whole structure at the transmission band because both layers are band-pass within the transmission band, while it can be absorbed by the lossy material at the absorption band.

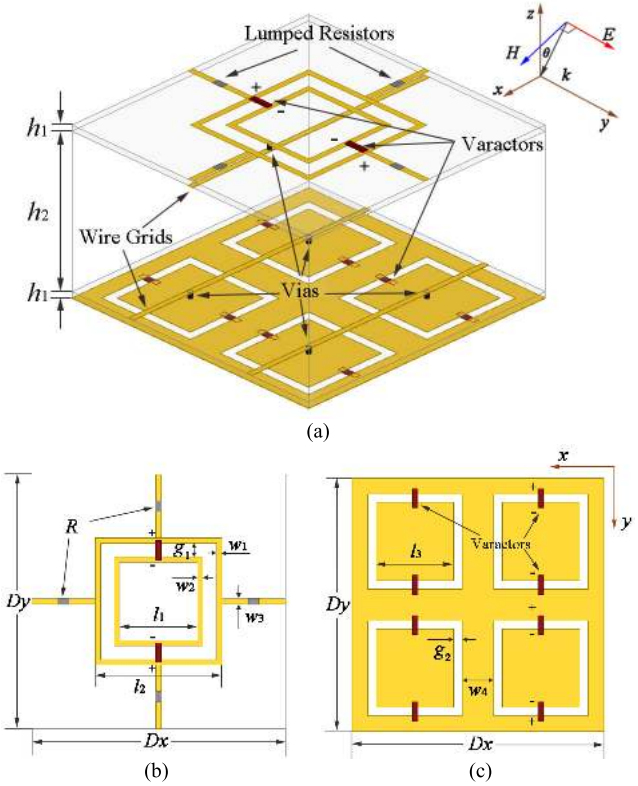

FIGURE 1. Geometry of the unit cell structure of the proposed FSR. (a) 3-D view of the FSR. (b) Top view of the lossy layer. (c) Top view of the bandpass layer.

In each unit cell of the tunable rasorber proposed in this paper, the lossy layer consists of a square-loop structure loaded with lumped resistors into four metallic strips. The lossless layer is a typical bandpass FSS. Copper patterns are printed on both layers that are separated by a dielectric spacer. The two FSS layers are separated by an intermediate air spacer. Furthermore, as shown in Fig. 1 (b) and (c), varactors on each layer are connected with the wire grid through metallic vias. Since all the varactors are biased in parallel, only a single RF choke is needed for RF/DC isolation. The dimensions of the unit cell along the x and y directions are specified by $D_x = D_y = D$ for the tunable FSR. The thickness and relative permittivity of the substrate are h_1 and ε_1, respectively.

B. EQUIVALENT CIRCUIT MODEL

In order to assist the design of our tunable FSR, an ECM is presented and analyzed in this subsection. Based on the ECM of a double square-loop and bandpass FSSs [33], the ECM of the proposed tunable FSR is constructed in Fig. 2. The lossy layer is mainly modeled by a series–parallel L_{c1}, C_c, and L_{c2} resonator, corresponding to the square-loop array. The resonator is then connected by two RC parallel resonators with the inductors L_s, which represents the strip lines around the square-loop. The values of inductors L_{c1} and L_{c2} are related to the side length of inner and outer loops, respectively. C_c is determined by the gap width g_1 between the two loops.

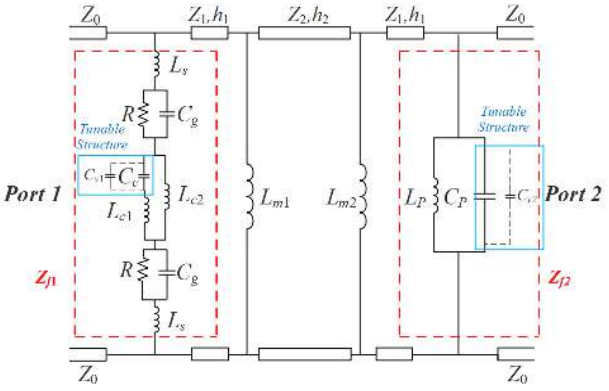

FIGURE 2. ECM of the proposed FSR.

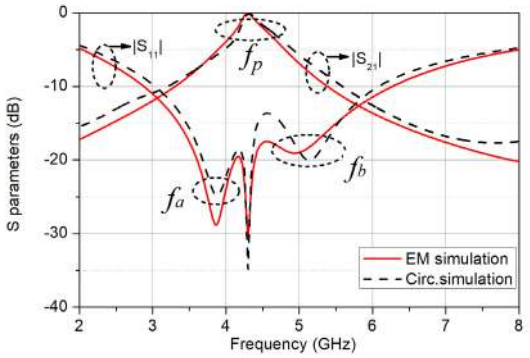

FIGURE 3. Comparison between S parameters of the FSR calculated from HFSS using periodic boundaries for normal incidence and the equivalent circuit model. (Circuit parameters: $Z_0 = Z_2 = 377\ \Omega$, $Z_1 = 236\ \Omega$, $R = 294\ \Omega$, $L_s = 3.2$ nH, $L_{c1} = 1.85$ nH, $L_{c2} = 2.05$ nH, $L_p = 3.9$ nH, $C_g = 0.06$ pF, $C_c = 0.34$ pF, $C_p = 0.35$ pF).

C_g is associated with the distance of the outer loops on the neighboring two units. The bandpass layer is modeled by a parallel L_pC_p resonator. The parallel inductors L_{m1} and L_{m2} model the inductive effect of the wire grid at the back of each layer. Z_0 and Z_1 represent the wave impedances of free space and substrate, respectively.

The surface impedances of the first and second layers are represented by Z_{f1} and Z_{f2}, respectively. According to [2], the surface impedances of the lossy FSS layer and lossless layer are:

$$Z_{f1} = 1/[j\omega C_c/(1-\omega^2 C_c L_{c1}) + 1/(j\omega L_{c2})] + 2^* j\omega L_s + 2/(j\omega C_g + 1/R) \quad (1)$$

$$Z_{f2} = 1/[j\omega C_p + 1/(j\omega L_p)] \quad (2)$$

where ω is the angular frequency.

At the transmission frequency f_p, to achieve a good transmission characteristic with low insertion loss, both impedances Z_{f1} and Z_{f2} should approach ∞. In this case, $|S_{11}| = 0$ and $|S_{21}| = 1$, which means that the incoming waves can propagate through the FSR from *Port 1* to *Port 2* with no absorption or loss. According to the ECM shown in Fig. 2, the resonant frequencies of the two FSSs are:

$$f_{p1} = \frac{1}{2\pi\sqrt{C_c(L_{c1}+L_{c2})}} \quad (3)$$

$$f_{p2} = \frac{1}{2\pi\sqrt{C_p L_p}} \quad (4)$$

Both the first and second layers must satisfy a parallel resonance at the same frequency, which means that $f_{p1} = f_{p2} = f_p$ for the center frequency of the transmission band.

At the absorption frequencies f_a and f_b, for an ideal FSR, $|S_{11}| = 0$ and $|S_{21}| = 0$. Based on the matrix conversion, the S matrix of the equivalent circuit network of the bandpass FSS layer can be obtained. The ABCD matrix of the cascaded two-port network for the air spacer and bandpass FSS can be written as:

$$\begin{bmatrix} A & B \\ C & D \end{bmatrix} = \begin{bmatrix} \cos\theta_2 & jZ_2\sin\theta_2 \\ jY_2\sin\theta_2 & \cos\theta_2 \end{bmatrix} \begin{bmatrix} 1 & 0 \\ Y_{f2} & 1 \end{bmatrix} \quad (5)$$

where $\theta_2 = 2\pi f h_2/c$, c is the speed of light, h_2 is the spacing between two substrates, and $Z_2 = 377\ \Omega$ is the free-space wave impedance. We may set $|S_{11}| = 0$ for an ideal FSR, and one can then solve:

$$\tan(\theta_2) = Z_2\left(\frac{1}{2\pi f L_p} - 2\pi f C_p\right) \quad (6)$$

for the designed frequencies f_a and f_b of the absorption bands.

In addition, the series resonant frequency f_s for the lossy FSS layer can be expressed as:

$$f_s = \frac{1}{2\pi\sqrt{C_c L_{c1}}} \quad (7)$$

where the series resonant frequency f_s is very close to the upper absorption frequency f_b. Under this situation, the connected resistors are providing the necessary absorption. It can be seen from Fig. 3 that the ECM results are in good agreement with the simulated ones using ANSYS HFSS, which verifies the validity of our proposed equivalent circuit.

It should be mentioned that the parallel inductances L_{M1} and L_{M2} introduced by the wire grids can have negligible influence. According to [30], one obtains

$$L_{Mi} = \mu_0\mu_{eff}\frac{P}{2\pi}\ln\left(\frac{1}{\sin(\pi W/(2D_i))}\right) \quad (i = 1, 2) \quad (8)$$

where W is the width of the wire grid, D_i is the size of each unit cell ($i = 1, 2$), μ_0 is the permeability of the vacuum and μ_{eff} is the effective relative permittivity of the substrate. The inductance embedded with wire grid can be calculated by:

$$L_{\text{lossless}} = 1/\left(1/L_P + 1/L_{M2}\right) = L_P/\left(1 + L_P/L_{M2}\right) \quad (9)$$

For the lossless FSS layer, we can obtain $L_{M2} = 57.3$ nH, which is much larger than the value of parameter L_P. When $L_{M2} >> L_P$, $L_{lossless}$ can be very close to L_P, indicating that the effect of L_{M2} can be ignored. The same conclusion applies to the lossy layer with L_{M1}.

C. TUNING MECHANISM

The proposed FSR structure can be simply modified to achieve a tunable response by loading varactors on the lossy and bandpass layers, as shown in Fig. 1(a). For the lossy layer, a metallic via and two varactors are included in each unit cell for tuning the resonant frequency. The varactors are inserted across the gap between the two square loops of the resonator. As shown in Fig. 1(b), the negative electrode of the varactors is on the inside of the square-loop, while the positive electrode moves towards outside. The strip lines around the square-loop are used to connect the positive electrode of varactors to the ground. The metallic via is used to connect the inner square loop to the back-bias wire electrically, providing the forward current to the negative electrode of the varactors. Furthermore, this structure can also reduce any voltage drop caused by the loss of the lumped resistors because the positive electrode is connected to the ground. With this design, the reverse bias voltage can be provided to the varactors synchronously. The same structure is also applied to the bandpass layer, as shown in Fig. 1(c).

By applying a DC bias voltage (V_b) between the two square loops, the equivalent capacitance between them can be varied electrically to realize a tunable frequency response on the lossy layer. With a proper design, the same tunable frequency response on the lossless layer can be supplied by the same bias voltage, resulting in a very simply tuning mechanism. As shown in Fig. 2, the equivalent capacitances of resonators on both layers can be defined as varactor capacitances C_{v1} and C_{v2}, respectively. The influence of the series resistance of the varactors we used will be discussed in the following sections. According to (1) and (2), we can obtain:

$$f_{p1}{}' = \frac{1}{2\pi\sqrt{(C_c + C_{v1})(L_{c1} + L_{c2})}} = f_{p2}{}' = \frac{1}{2\pi\sqrt{(C_p + C_{v2})L_p}} = f_p{}' \tag{10}$$

where $f_{p1}{}'$ and $f_{p2}{}'$ are tunable resonator frequencies with varied capacitances.

In addition, the absorption rate of the tunable FSR is defined as the percentage of energy absorbed by the lossy layer, which is calculated as:

$$Absorption = 1 - |S_{11}|^2 - |S_{21}|^2 \tag{11}$$

D. DESIGN OF THE TUNABLE RASORBER

According to the ECM and tuning mechanism discussed above, the transmission band f_p is mainly determined by the resonant frequencies of both FSSs. Based on the ECM and the conducted analysis, the design guidelines can be formulated and a tunable FSR can then be quickly designed as follows.

1) As shown in Fig. 3, the frequency f_p is assumed to be the transmission frequency of the absorber to be designed. The thickness h_2 of the air spacer between the two FSSs can be evaluated similar to the Salisbury screen [4], which is $2\beta_1 h_1 + \beta_2 h_2 = \pi/2$, $\beta_i = 2\pi/\lambda_i$, $i = 1, 2$. $\lambda$is the wavelength of the EM wave propagating in different dielectric media. Furthermore, the thickness of the air spacer can be reduced by selecting a substrate with higher dielectric constant for the spacer, although it may result in a narrower transmission bandwidth.
2) For the unit cell of the FSSs, $D_x = D_y < \lambda_p/2$. Based on the ECM, according to the desired transmission frequency (f_p) and absorption frequencies (f_a and f_b), a quick optimization can be carried out to determine the equivalent resistances, inductances, and capacitances of the square-loop as well as the bandpass structure.
3) The equivalent inductance L and capacitance C are determined by a function F given in [3]. It is clear that the values of the gaps (g_1 and g_2) must be suitable for the size of varactors we used, which means that g_1 and g_2 can be decided based on the provided dimensions of the varactors. The physical dimensions of the two FSSs can then be estimated by the formulas provided in [30] and [34]. It should be mentioned that the functions are mainly related to frequency f_p. In order to obtain a quick design, the physical lengths l_2 and l_3 related to the lossless slot may be set as $l_2 \approx l_3 \approx 0.25c/f_p$.
4) Based on transmission line theory, the desirable frequency responses of the FSR can be obtained through a quick circuit simulation with the combination of selected resistors. It should be noted that a large absorption bandwidth can be realized by properly choosing the values of the inserted resistors.
5) Based on the estimated dimensions from the analysis of the tunable FSR, the full-wave simulators, ANSYS HFSS and CST Microwave Studio, can be used to further optimize the structure for better accuracy.

The guidelines above can provide considerable design flexibility and a fast optimization procedure.

In this paper, a design example is fabricated and tested. The original desirable transmission frequency is $f_p = 5.2$ GHz. More specifically, the substrate material used for fabrication is Rogers 4003, with a dielectric constant $\varepsilon_1 = 3.55$ and thickness $h_1 = 0.508$ mm. Since the original center transmission frequency is 5.2 GHz, we obtain $h_2 = 13.6$ mm for the ideal air spacer with $\varepsilon_2 = 1$. As shown in Fig. 1, the final dimensions are: $l_1 = 7.6$ mm, $l_2 = 10.2$ mm, $l_3 = 9.7$ mm, $w_1 = w_2 = w_3 = 0.5$ mm, $w_4 = 1.7$ mm, $g_1 = g_2 = 0.3$ mm, $D_x = D_y = 24$ mm, $R = 294\ \Omega$. The used varactor is MA46H120, which is a GaAs flip-chip diode and it can provide a tunable range of capacitance from 0.12 to 1.00 pF for a reverse bias voltage between 16 and 0 V. The fabricated sample of the lossy layer also consists of four lumped resisters in each unit cell with a value of 294 Ω. The resonators in the front and back layers of the tunable FSR are connected to the bias wire grid through vias of 0.3 mm diameter.

It should be mentioned that in this work, only a single polarization of the incident wave (TE polarization) is considered, as shown in the Fig. 1(a). We have designed the direction of the biasing wire grid along the x-axis, perpendicular to the E-field direction of the TE wave. The width of the bias

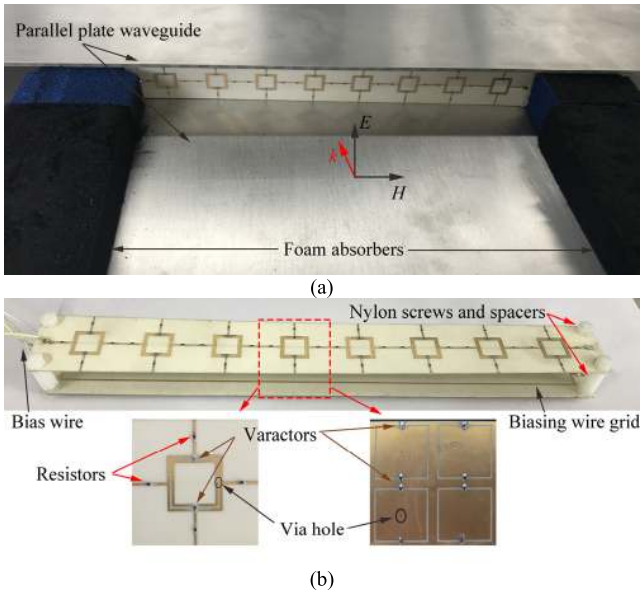

FIGURE 4. Measurement setup of proposed structure and assembly details. (a) FSR measurement setup inside the parallel-plate waveguide (PPW) testing platform. (b) 3-D view of the fabricated tunable FSR sample and details of the unit cell.

wire grid is 0.5 mm along the *y*-axis direction, which is relatively small. The effect of the biasing wire grid has been investigated and it is found to be negligible.

III. EXPERIMENTAL RESULTS AND DISCUSSION

A photograph of our fabricated tunable FSR prototype consisting of eight cells in one direction with the size of 24×196 mm^2 is shown in Fig. 4, with several supporting plastic nylon screws and spacers, which maintains a uniform gap of 14 mm. The designed FSR has been measured inside a parallel-plate waveguide (PPW) setup [4], as shown in Fig. 4(a). The setup cell supports a TEM wave propagation, which can mimic a free-space environment approximately. The biasing wire grids on each layer are connected to a variable DC power supply. In this way, all the varactors are reverse-biased, and their capacitance can be tuned continuously by changing the DC bias voltage. A 40-kΩ resistor is connected to the wire grid to act as an RF choke [30]. In the measurements, the bias voltage is firstly set to 16 V to test the lowest capacitance value of 0.12 pF for each varactor, corresponding to a center transmission frequency of 5.2 GHz for the transmission band. The bias voltage is then decreased step-by-step from 16 to 4 V with a step size of 2 V, and the variation of the transmission responses is recorded for each step.

The comparison of the simulated and measured reflection and transmission coefficients of the tunable FSR under the normal incidence is shown in Fig. 5. It can be clearly noticed that the simulation and experiment results are in good agreement. The bias voltage in the measurement is decreased from 16 to 4 V gradually, while the capacitor value can be tuned from the lowest 0.12 pF to the highest 0.38 pF, corresponding to a change of the center transmission frequency from

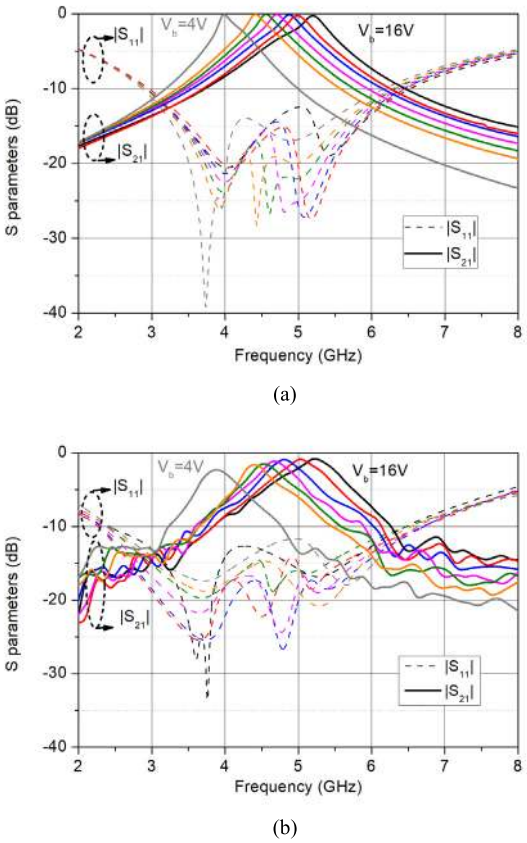

FIGURE 5. Reflection and transmission responses of the designed tunable FSR under normal incidence for different values of varactor bias voltage. The reverse bias voltage (V_b) is varied from 16 to 4 V with a step size of 2 V. (a) Results obtained from EM simulations. (b) Measured reflection and transmission responses.

5.2 to 3.8 GHz simultaneously. The measured insertion loss is less than 0.59 dB at 5.2 GHz when the bias voltage equals to 16 V, while the fractional bandwidth for reflection less than −10 dB is 93.1% (2.4–6.58 GHz). When the bias voltage equals to 4 V, the fractional bandwidth for reflection less than −10 dB is 96.7% (2.26-6.49GHz). The intermediate performance have similar results. Meanwhile, a frequency shift of less than 0.1 GHz at the lower band is observed when comparing with the simulated results, which is probably caused by the variation of component values and the parasitic effects of the lumped elements. It should be mentioned that the measured insertion loss is less than 2.5 dB at the lower band, which is bigger than the simulated one. This is mostly due to the ohmic loss of the varactors. The passband is defined as the bandwidth with −3 dB from the peak of the transmission response. And the fractional bandwidth for this passband is 15.4% when the bias voltage is at 16 V. The insertion loss increases as the bias voltage is decreased because the varactor exhibits a larger series resistance at a lower bias voltage. Fig. 6(a) illustrates the variation of the series parasitic resistance of the varactor as a function of the reverse bias voltage. The center frequency of the FSR and the varactor capacitance versus the bias voltage are plotted in Fig. 6(b). The variation of the center frequency is not smooth

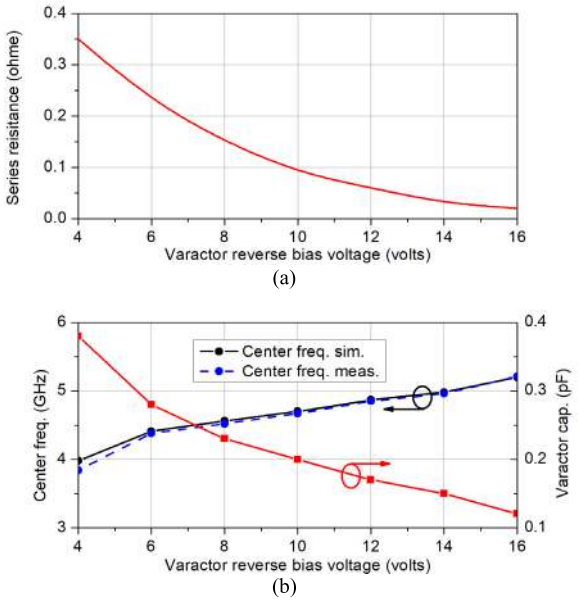

FIGURE 6. (a) Series resistance of the varactor as a function of the reverse bias voltage. (b) Variation of the varactor diode capacitance and the center frequency of the tunable FSR as a function of the reverse bias voltage.

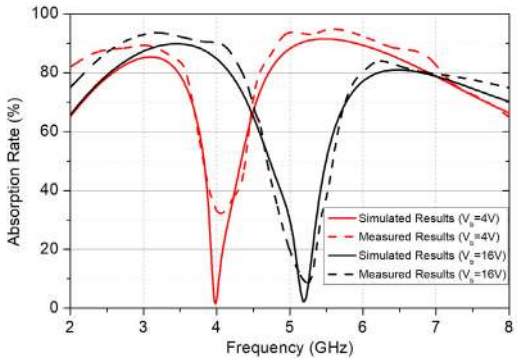

FIGURE 7. Comparison of the EM simulated and measured absorption rate results.

when the voltages decreases due to the nonlinear relationship between the varactor capacitance and the bias voltage.

Fig. 7 illustrates the EM simulation and experiment results of the absorption rate at the upper and lower limits of the tuning band. It is shown that at the upper limit when the bias voltage equals to 16 V, the FSR has more than 90% absorption for an incident EM wave from 2.76 to 3.95 GHz, which represents a bandwidth of 35.5%. When the bias voltage equals to 4 V, the 90% absorption band is from 4.8 to 6.25 GHz with the fractional bandwidth of 26.2%. The absorption band shifts to the high frequency band as the voltage decreases. The measured absorption bandwidths are slightly larger than the simulated ones, which is mainly due to the ohmic loss of the varactors and the parasitic effect of the used lumped resistors.

The sensitivity of the tunable FSR's responses on the oblique incidences of the plane EM wave is further explained

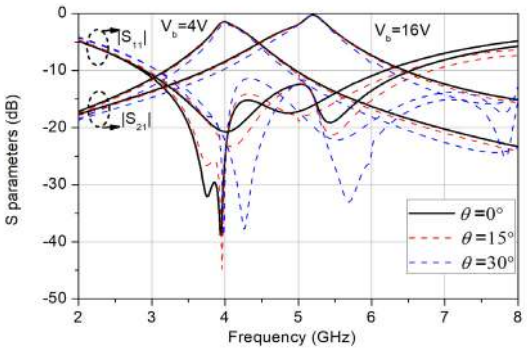

FIGURE 8. Simulated reflection coefficient and transmission coefficient of the proposed FSR unit cell under an oblique incidence.

TABLE 1. Comparisons between conventional FSR/FSS and proposed tunable FSR.

Reference	Insertion Loss (dB)	FBW ($\|S_{11}\| < -10$dB)	Tunable range	Thickness (λ_L)	FSR/FSS
[17]	0.5	108%	N.A	0.19	FSR
[21]	0.68	92.3%	N.A	0.108	FSR
[22]	< 1	80%.	17.8%	N.A	FSR
[31]	3.3	95%	33%	N.A	FSR
[32]	0.64	99.6%	Switchable	0.09	FSR
[26]	< 1	N.A.	6%	N.A	FSS
Our work	0.59	93.1%	31%	0.107	FSR

in Fig. 8 through EM simulations. The scan plane of oblique incidence angle θ is located in the yz plane for TE wave. The results provided for the upper and lower limits of the tuning band demonstrate that the designed FSR exhibits a stable response in the range of the incident angles up to 30°. This stability is mainly due to the relatively small dimension of the unit cell.

In order to better understand the advantages of our tunable structure, a comparison with other reported designs in the literature is made and provided in Table I. It can be obviously seen that a continuous tunable range has been obtained and developed while the thickness and insertion loss of our design are relatively small. The fractional bandwidth for reflection less than -10 dB is around 93%, which is relatively large. In addition, the topology of our design is polarization-sensitive for TE wave only because the varactors are only inserted along the y-axis, as we have discussed in Section II. The current design can be further generalized to suit dual polarizations (both TE and TM waves) if the varactors are assembled along both x-axis and y-axis. In this situation, the effect of the biasing networks should be more carefully characterized and compensated.

IV. CONCLUSION

A tunable FSR based on square-loop array has been successfully designed and verified at the microwave band.

The tunability is achieved by integrating varactors on both lossy and lossless layers. An ECM is given to analyze the operating principle and design guidelines based on the ECM has then been developed. The unique feature of our proposed structure is that all the varactors are biased by embedded wire grid through metallic vias resulting in a low insertion loss, broadband, and high-selectivity rasorber. Measured results show that the designed rasorber has a continuous tuning range from 5.2 to 3.8 GHz for the center transmission frequency when the bias voltage changes from 16 to 4 V. Furthermore, the structure can be readily generalized to dual-polarized rasorber. Owing to the low insertion loss feature and tunable transmission band, the proposed FSR has potential applications in tunable and reconfigurable stealthy antenna-radome systems.

REFERENCES

[1] B. A. Munk, *Metamaterials: Critique and Alternatives*. Hoboken, NJ, USA: Wiley, 2009.
[2] B. A. Munk, *Frequency Selective Surfaces: Theory and Design*. Hoboken, NJ, USA: Wiley, 2005.
[3] N. Marcuvitz, *Waveguide Handbook*. New York, NY, USA: McGraw-Hill, 1951.
[4] Y. Shang, Z. Shen, and S. Xiao, "On the design of single-layer circuit analog absorber using double-square-loop array," *IEEE Trans. Antennas Propag.*, vol. 61, no. 12, pp. 6022–6029, Dec. 2013.
[5] G. I. Kiani, K. L. Ford, K. P. Esselle, A. R. Weily, and C. J. Panagamuwa, "Oblique incidence performance of a novel frequency selective surface absorber," *IEEE Trans. Antennas Propag.*, vol. 55, no. 10, pp. 2931–2934, Oct. 2007.
[6] F. Costa and A. Monorchio, "A frequency selective radome with wideband absorbing properties," *IEEE Trans. Antennas Propag.*, vol. 60, no. 6, pp. 2740–2747, Jun. 2012.
[7] U. Rafique, G. I. Kiani, M. M. Ahmed, and S. Habib, "Frequency selective surface absorber for WLAN security," in *Proc. 5th Eur. Conf. Antennas Propag.*, Apr. 2011, pp. 872–875.
[8] Z. Wang, Q. Zeng, J. Fu, W. Chen, B. Lv, M. Song, and T. A. Denidni, "A high-transmittance frequency-selective rasorber based on dipole arrays," *IEEE Access*, vol. 6, pp. 31367–31374, 2018.
[9] Z. Sun, Q. Chen, M. Guo, H. Yu, and Y. Fu, "Frequency selective rasorber and reflector with two-sided absorption bands," *IEEE Access*, vol. 7, pp. 6025–6031, Dec. 2018.
[10] M. Guo, Z. Sun, D. Sang, X. Jia, and Y. Fu, "Design of frequency-selective rasorbers based on centrosymmetric bended-strip resonator," *IEEE Access*, vol. 7, pp. 24964–24970, Jan. 2019.
[11] Y. Zhang, B. Li, L. Zhu, Y. Tang, Y. Chang, and Y. Bo, "Frequency selective rasorber with low insertion loss and dual-band absorptions using planar slotline structures," *IEEE Antennas Wireless Propag. Lett.*, vol. 17, no. 4, pp. 633–636, Apr. 2018.
[12] S. Zhong, L. Wu, T. Liu, J. Huang, W. Jiang, and Y. Ma, "Transparent transmission-selective radar-infrared bi-stealth structure," *Opt. Express*, vol. 26, no. 13, pp. 16466–16476, Jun. 2018.
[13] Q. Chen and Y. Fu, "An absorptive frequency selective surface with wideband transmission above absorption band," in *Proc. IEEE Int. Symp. Antennas Propag. USNC/URSI Nat. Radio Sci. Meeting*, Jul. 2017, pp. 685–686.
[14] Q. Chen, S. Yang, J. Bai, and Y. Fu, "Design of absorptive/transmissive frequency-selective surface based on parallel resonance," *IEEE Trans. Antennas Propag.*, vol. 65, no. 9, pp. 4897–4902, Sep. 2017.
[15] S. Hamid, B. Karnbach, H. Shakhtour, and D. Heberling, "Thin multilayer frequency selective surface absorber with wide absorption response," in *Proc. Loughborough Antennas Propag. Conf.*, Nov. 2015, pp. 1–5.
[16] H. Wakatsuchi, D. F. Sievenpiper, and C. Christopoulos, "Designing flexible and versatile metamaterial absorbers," *IEEE Electromagn. Compat. Mag.*, vol. 5, no. 2, pp. 76–82, 2nd Quart., 2016.
[17] Z. Shen, J. Wang, and B. Li, "3-D frequency selective rasorber: Concept, analysis, and design," *IEEE Trans. Microw. Theory Techn.*, vol. 64, no. 10, pp. 3087–3096, Oct. 2016.
[18] A. A. Omar, Z. Shen, and H. Huang, "Absorptive frequency-selective reflection and transmission structures," *IEEE Trans. Antennas Propag.*, vol. 65, no. 11, pp. 6173–6178, Nov. 2017.
[19] Y. Yu, G. Q. Luo, Q. Liu, W. Yu, H. Jin, Z. Liao, and Z. Shen, "3D band-absorptive frequency selective rasorber: Concept and analysis," *IEEE Access*, vol. 7, pp. 2520–2528, 2018.
[20] T. Deng, Y. Yu, and Z. N. Chen, "A broadband 3D frequency selective rasorber by using magnetic materials," in *Proc. Int. Conf. Electromagn. Adv. Appl. (ICEAA)*, Verona, Italy, Sep. 2017, pp. 1731–1734.
[21] Y. Shang, Z. Shen, and S. Xiao, "Frequency-selective rasorber based on square-loop and cross-dipole arrays," *IEEE Trans. Antennas Propag.*, vol. 62, no. 11, pp. 5581–5589, Nov. 2014.
[22] A. A. Omar and Z. Shen, "Tunable absorptive frequency-selective transmission structure," in *Proc. Int. Symp. Antenna Propag. USNC/URSI Nat. Radio Sci. Meeting*, Jul. 2018, pp. 2063–2064.
[23] S. N. Azemi, K. Ghorbani, and W. S. T. Rowe, "A reconfigurable FSS using a spring resonator element," *IEEE Antennas Wireless Propag. Lett.*, vol. 12, pp. 781–784, 2013.
[24] B. Schoenlinner, A. Abbaspour-Tamijani, L. C. Kempel, and G. M. Rebeiz, "Switchable low-loss RF MEMS Ka-band frequency-selective surface," *IEEE Trans. Microw. Theory Techn.*, vol. 52, no. 11, pp. 2474–2481, Nov. 2004.
[25] T. K. Chang, R. J. Langley, and E. A. Parker, "Frequency selective surfaces on biased ferrite substrates," *Electron. Lett.*, vol. 30, no. 15, pp. 1193–1194, Jul. 1994.
[26] A. Ebrahimi, P. Yaghmaee, W. Withayachumnankul, C. Fumeaux, S. Al-Sarawi, and D. Abbott, "Interlayer tuning of X-band frequency-selective surface using liquid crystal," in *Proc. Asia–Pacific Microw. Conf. (APMC)*, Nov. 2013, pp. 1118–1120.
[27] C. Mias, "Varactor-tunable frequency selective surface with resistive-lumped-element biasing grids," *IEEE Microw. Wireless Compon. Lett.*, vol. 15, no. 9, pp. 570–572, Sep. 2005.
[28] X. G. Huang, Z. Shen, Q. Y. Feng, and B. Li, "Tunable 3-D bandpass frequency-selective structure with wide tuning range," *IEEE Trans. Antennas Propag.*, vol. 63, no. 7, pp. 3297–3301, Jul. 2015.
[29] A. Ebrahimi, W. Withayachumnankul, S. F. Al-Sarawi, and D. Abbott, "Higher-order tunable frequency selective surface with miniaturized elements," in *Proc. 15th Medit. Microw. Symp.*, Nov./Dec. 2015, pp. 1–4.
[30] A. Ebrahimi, Z. Shen, W. Withayachumnankul, S. F. Al-Sarawi, and D. Abbott, "Varactor-tunable second-order bandpass frequency-selective surface with embedded bias network," *IEEE Trans. Antennas Propag.*, vol. 64, no. 5, pp. 1672–1680, May 2016.
[31] Y. Han, W. Che, X. Xiu, W. Yang, and C. Christopoulos, "Switchable low-profile broadband frequency-selective rasorber/absorber based on slot arrays," *IEEE Trans. Antennas Propag.*, vol. 65, no. 12, pp. 6998–7008, Dec. 2017.
[32] L. Wu, S. Zhong, J. Huang, and T. Liu, "Broadband frequency-selective rasorber with varactor-tunable inter-absorption band transmission window," *IEEE Trans. Antennas Propag.*, to be published.
[33] H. Huang and Z. Shen, "Absorptive frequency-selective transmission structure with square-loop hybrid resonator," *IEEE Antennas Wireless Propag. Lett.*, vol. 16, pp. 3212–3215, 2017.
[34] Y. Han, W. Che, C. Christopoulos, Y. Xiong, and Y. Chang, "A fast and efficient design method for circuit analog absorbers consisting of resistive square-loop arrays," *IEEE Trans. Electromagn. Compat.*, vol. 58, no. 3, pp. 747–757, Jun. 2016.

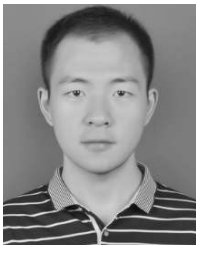

YIHAO WANG was born in Shannxi, Xian, China, in 1992. He received the B.Eng. degree from the School of Electronic and Information Engineering, Beihang University, Beijing, China, in 2014. He is currently pursuing the Ph.D. degree in information and communication engineering with the School of Electronic and Optical Engineering, Nanjing University of Science and Technology, China.

His current research interests include microwave circuit analog absorber, frequency selected surface, and absorber measurement.

SHI-SHAN QI (M'13) was born in Shandong, China, in 1983. He received the B.S. degree in electronic information engineering and the Ph.D. degree in communications and information systems from the Nanjing University of Science and Technology, Nanjing, China, in 2005 and 2012, respectively, where he has been an Associate Professor with the School of Electronic and Optical Engineering, since 2016.

His current research interests include conical beam antenna, reconfigurable water antennas, wireless power transmission, and microwave- and millimeter-wave theories and technologies.

ZHONGXIANG SHEN (M'98–SM'04–F'17) received the B.Eng. degree in electrical engineering from the University of Electronic Science and Technology of China, Chengdu, China, in 1987, the M.S. degree in electrical engineering from Southeast University, Nanjing, China, in 1990, and the Ph.D. degree in electrical engineering from the University of Waterloo, Waterloo, ON, Canada, in 1997.

From 1990 to 1994, he was with the Nanjing University of Aeronautics and Astronautics, Nanjing. He joined Com Dev Ltd., Cambridge, ON, as an Advanced Member of Technical Staff, in 1997. In 1998, he joined the Gordon McKay Laboratory, Harvard University, Cambridge, MA, USA, and the Radiation Laboratory, University of Michigan, Ann Arbor, MI, USA, as a Postdoctoral Fellow. In 1999, he joined Nanyang Technological University, Singapore, as an Assistant Professor, where he is currently a Full Professor. He has authored or coauthored over 170 journal papers, among them 100 were published in IEEE journals, and presented over 160 conference papers. His current research interests include the design of small and planar antennas for various wireless communication systems, analysis and design of frequency-selective structures, and hybrid numerical techniques for modeling RF/microwave components and antennas.

Dr. Shen served as the Chair of the IEEE MTT/AP Singapore Chapter, in 2009. He was the Chair of the IEEE AP-S Chapter Activities Committee, from 2010 to 2014. He is currently the Secretary of the IEEE AP-S and an Associate Editor of the IEEE TRANSACTIONS ON ANTENNAS AND PROPAGATION.

WEN WU (SM'10) received the Ph.D. degree in electromagnetic field and microwave technology from Southeast University, Nanjing, China, in 1997.

He is currently a Professor with the School of Electronic Engineering and Optoelectronic Technology, Nanjing University of Science and Technology, Nanjing, where he is also an Associate Director with the Ministerial Key Laboratory, JGMT. He has authored or coauthored over 60 journal and conference papers and has submitted 5 patent applications. His current research interests include microwave and millimeter-wave theories and technologies, microwave and millimeter-wave detection, and multimode compound detection.

Dr. Wu was a recipient of six times of the Ministerial and Provincial-Level Science and Technology Awards.